Effect of the Damper between Maglev Vehicles on Curve Negotiation

Ki-Jung Kim, Hyung-Suk Han and Chang-Hyun Kim
KIMM, Dept. of Magnetic Levitation and Linear Drive, Daejeon 305-343, KOREA
kkj74@kimm.re.kr, hshan@kimm.re.kr,chkim78@kim.re.kr

Nam-Jin Lee
Advanced Vehicle Development Team, Rotem Company, Korea
njlee@hyundai-rotem.co.kr

ABSTRACT: In the magnetic train composed of more than two cars, the installation of the dampers between cars is carefully considered for improving both ride and safety especially in curve. Dynamic simulation of ride and curving of the Maglev vehicle under test is carried out. The dynamic model is developed based on multibody dynamics. With the model, the effects of the dampers are numerically analyzed. The damping properties are suggested based on the results from the simulation. The proposed damper is installed to the vehicle and tested to confirm the effects. In this paper, the simulation and measured results on the vehicle dynamics and ride quality are discussed.

1 INTRODUCTION

Korea Institute of Machinery and Materials (KIMM), in cooperation with ROTEM Co, have conducted the evaluation test mainly to confirm the safety and reliability of the Maglev vehicle, which is developed by Korea's Urban Maglev Program.

As reported previous study [1], ride quality and curving performance of urban transit Maglev is already felt to be a reasonable level. However, although the ride quality of urban transit Maglev was considered to be allowable for transportation, yawing motion of vehicles was observed during running through the curved guideway. So it is essential to reduce yawing motion and lateral vibration to coincide with advantages of urban transient Maglev such as high ride quality and availability to travel along short curve.

The installment of yaw damper to solve such those may decrease the safety of the maglev vehicle while running curves because it is believed that the independency between vehicles of maglev is relatively larger than that of wheel-on-rail.

In this paper, a full vehicle multibody dynamic model including integration of the electromagnet model and its control algorithm is presented, dynamic behaviors of the Maglev vehicles are analyzed to evaluate effect of damper connecting two vehicles to improve ride quality and curve negotiation performance throughout dynamic simulation and test.

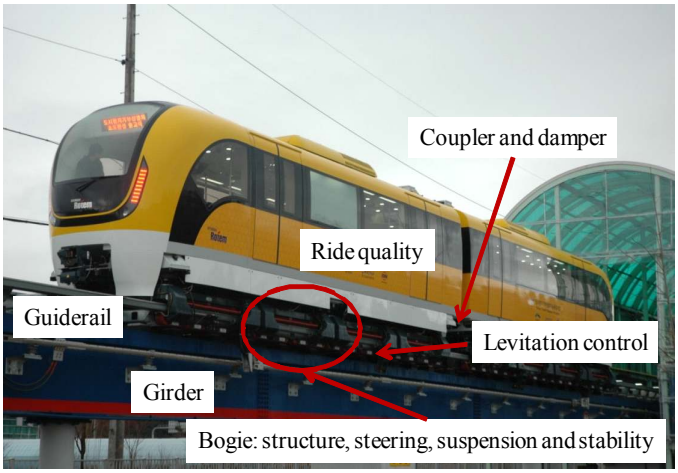

Figure 1. Maglev under test

2 MODELING

2.1 Curved guideway

The curved guideway is composed of the tangent, transition and circular curve sections. The minimum length of the transition section is limited by the allowed superelevation gradient, which is determined by the mechanical decoupling tolerance and the guideway cant is incrementally increased to a specified angle. In the test track at KIMM, 30m-length clothoid transition section and 38 cant angle is arranged for the 180m-radius curve, but 200m-radius curve instead of transition section is arranged for the 60m-radius curve.

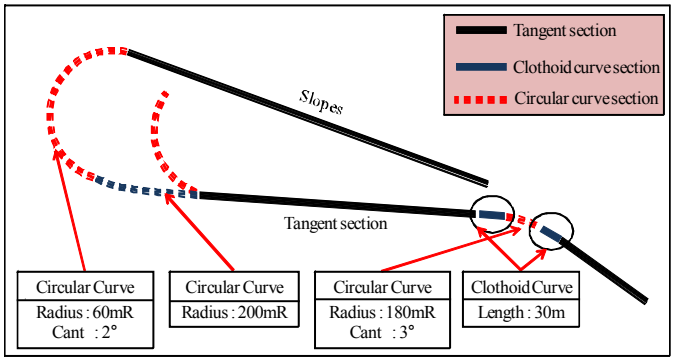

Figure 2. Test track at KIMM

2.2 Dynamic model

A full vehicle multibody dynamic model, as shown in Figure 3, which can be more realistically predict and accurately evaluate the dynamic responses of Maglev vehicle is described in the following.

Each carbody has 4 bogies and is supported vertically on the sliding table. Each bogie consists of right and left modules, and linked with each other using four pieces of antiroll beams. Modules and sliding table are relatively movable in the lateral direction but to a limited extent due to four air springs mounted in between in parallel which have lateral stiffness. 8 electromagnets are attached to modules of the bogie for levitation and guidance. Each module has two electromagnets on a corner and is controlled independently by changing the voltage in their winding. The forces generated by the electromagnets are described in the section 2.4 in detail.

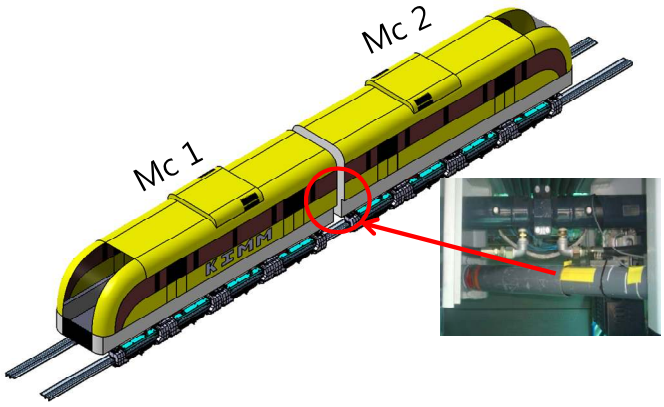

Figure 3. Dynamic full car model connected with damper

In the simulation, TSDA (Translational Spring Damper Actuator) force element is used to represent damper model. Here, only a value of damping defines the TSDA force, and the damping force is defined by a curve as shown in Figure 4.

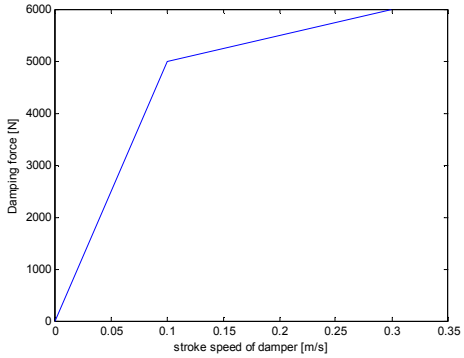

Figure 4. Characteristics of damper

2.3 Axis system

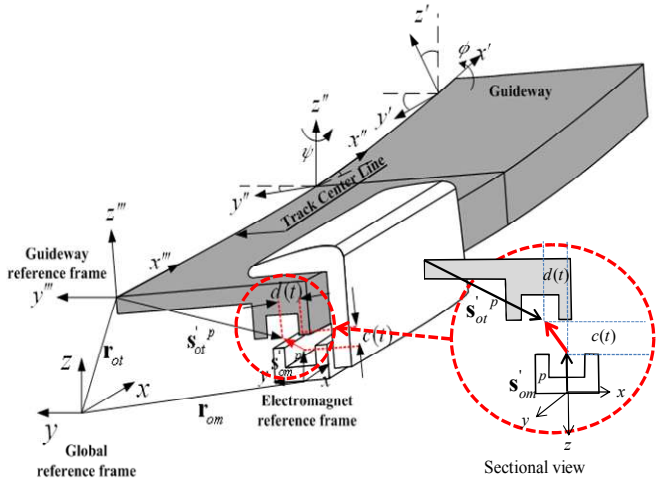

Figure 5. Track coordinate

The definitions of the vertical air gap, $c(t)$, and the lateral air gap, $d(t)$, are illustrated in Figure 5. The vector between the electromagnet and guiderail is in the global reference frame as

$$\boldsymbol{r}_{tm} = \boldsymbol{r}_t - \boldsymbol{r}_m = \boldsymbol{r}_{0t} + \boldsymbol{A}_t \boldsymbol{s}'^{\,p}_{0t} - \boldsymbol{r}_{0m} - \boldsymbol{A}_m \boldsymbol{s}'^{\,p}_{0m} \tag{1}$$

The transformation matrix $\boldsymbol{A}_t$ from the guideway to the global reference frame has the form

$$\boldsymbol{A}_t = \begin{bmatrix} \cos\psi & -\sin\psi & 0 \\ \cos\varphi\sin\psi & \cos\varphi\cos\psi & -\sin\varphi \\ \sin\varphi\sin\psi & \sin\varphi\cos\psi & \cos\varphi \end{bmatrix} \tag{2}$$

$\boldsymbol{A}_t$ can be geometrically predefined along the center line of the guideway to be considered. On the other hand, $\boldsymbol{A}_m$ is temporally determined by the generalized orientation coordinates of the electromagnet. When the Euler parameters are used for orientation, $\boldsymbol{A}_m$ is defined as

$$\boldsymbol{A}_m = 2\times \begin{bmatrix} e_0^{\,2} + e_1^{\,2} - \frac{1}{2} & e_1e_2 - e_0e_3 & e_1e_3 + e_0e_2 \\ e_1e_2 + e_0e_3 & e_0^{\,2} + e_1^{\,2} - \frac{1}{2} & e_2e_3 - e_0e_1 \\ e_1e_3 - e_0e_2 & e_2e_3 + e_0e_1 & e_0^{\,2} + e_1^{\,2} - \frac{1}{2} \end{bmatrix} \tag{3}$$

where

e_0, e_1, e_2, e_3: *Euler parameters.*

The x-axis of the reference frame moves along the center line of the guideway, and the y-axis is perpendicular to the center line, as shown in Figure 5. Here, it is assumed that the reference frame can only rotate around two axes with respect to the global reference frame. First, the guideway reference frame rotates the angle φ around the z-axis of the global reference frame. Next, the new guideway reference frame rotates the angle ψ around the x-axis itself. Here, the rotation angle ψ represents the cant of the guideway.

2.4 Equations of motion and solution

The system governing equations, which are the system equations of motion, are formed by combining the dynamic equations for the vehicle in the form of mixed DAE (differential-algebraic equations) with the equations for the electromagnet and its control system in the form of ODE (ordinary differential equations). The equations of motion for the vehicle, a constrained mechanical system, are the following:

$$\begin{bmatrix} \mathbf{M} & \mathbf{\Phi_q}^{\mathbf{T}} \\ \mathbf{\Phi_q} & \mathbf{0} \end{bmatrix} \begin{bmatrix} \ddot{\mathbf{q}} \\ \boldsymbol{\lambda} \end{bmatrix} = \begin{bmatrix} \mathbf{Q} \\ \boldsymbol{\gamma} \end{bmatrix} \tag{4}$$

$$\mathbf{\Phi}(\mathbf{q}, t) = \left[\mathbf{\Phi}_1(\mathbf{q}, t), \cdots\cdots \mathbf{\Phi}_m(\mathbf{q}, t)\right]^T = \mathbf{0} \tag{5}$$

$$\mathbf{\Phi_q}\dot{\mathbf{q}} = -\mathbf{\Phi}_t \equiv \nu \tag{6}$$

$$\mathbf{\Phi_q}\ddot{\mathbf{q}} = -(\mathbf{\Phi_q}\dot{\mathbf{q}})_{\mathbf{q}}\,\mathbf{q} - 2\mathbf{\Phi}_{\mathbf{qt}}\dot{\mathbf{q}} - \mathbf{\Phi}_{tt} \equiv \boldsymbol{\gamma} \tag{7}$$

where $\boldsymbol{q}(t)$ is the position, $\dot{\boldsymbol{q}}(t)$ the velocity, $\ddot{\boldsymbol{q}}(t)$ the acceleration, $\boldsymbol{M}(t)$ the mass matrix, $\mathbf{\Phi_q}(t) \equiv \left[\partial \mathbf{\Phi}_j / \partial \mathbf{\Phi}_i\right]_{m\times n}$ the constraint Jacobean, $\boldsymbol{Q}(t)$ the external force, $\boldsymbol{\lambda}(t)$ the Lagrange multiplier. The levitation and guidance forces are added to the right side of Equation 3 and expressed as

$$F_0(\Delta c(t), \Delta i(t)) = k_c \Delta c(t) - k_i \Delta i(t) + F_{static} \tag{8}$$

$$F_z = F_0 \times \left[1 + \frac{2c(t)}{\pi\omega_m} + \frac{2d(t)}{\pi\omega_m}\tan^{-1}\left(\frac{c(t)}{d(t)}\right)\right] \tag{9}$$

$$F_y = F_0 \times \left[-\frac{2c(t)}{\pi\omega_m}\tan^{-1}\left(\frac{c(t)}{d(t)}\right)\right] \tag{10}$$

where, F_0 is the linearized levitation force around the nominal equilibrium point (i_0, c_0), F_y the guidance force, F_z the levitation force, d the lateral gap, c the air gap, and W_m the magnet width.

On the other hand, current changes are expressed as Equation 10. This equation for the electromagnet is incorporated into the equations for the vehicle mentioned above.

$$\Delta\dot{i}(t) = \frac{k_c}{k_i}\Delta\dot{c}(t) - \frac{R}{L_0}\Delta i(t) + \frac{1}{L_0}\Delta v(t) \tag{11}$$

where

$$L_0 = \frac{\mu_0 N^2 A}{2c_0}, \quad k_i = \frac{\mu_0 N^2 A i_0}{2c_0^{\,2}}, \quad k_c = \frac{\mu_0 N^2 A i_0^{\,2}}{2c_0^{\,3}} \quad ,$$

and A the section area, μ_0 the permeability, c_0 the nominal air gap, v the voltage, R the resistance and N the number of turn of magnet coil.

Using the control law, the controlled voltage is determined by

$$\begin{aligned} \Delta v(t) = {} & k_1 \Delta\hat{\ddot{z}}(t) + k_2 \Delta\hat{\dot{z}}(t) + k_3 \Delta\hat{z}(t) \\ & + k_4 \Delta\hat{\dot{c}}(t) + k_5 \Delta\hat{c}(t) \end{aligned} \tag{12}$$

where $\Delta\hat{\ddot{z}}(t)$ is the observed acceleration, $\Delta\hat{\dot{z}}(t)$ the observed velocity, $\Delta\hat{z}(t)$ the observed position, $\dot{c}(t)$ the observed air gap, $c(t)$ the observed air gap,

and k_1, k_2, k_3, k_4, k_5 are control gains.

Only two states, the acceleration of the electromagnet $\Delta\hat{\ddot{z}}(t)$ and air gap $c(t)$, used in the paper since it is practically difficult to measure all the five states. Equation 12 and 13 are the equations of state []. Both equations are also incorporated into the equations for the vehicle mentioned above.

$$\begin{bmatrix} \dot{x}_1(t) \\ \dot{x}_2(t) \\ \dot{x}_3(t) \\ \dot{x}_4(t) \\ \dot{x}_5(t) \end{bmatrix} = \begin{bmatrix} 0 & \frac{1}{T_3} & 0 & \frac{1}{T_3} & 0 \\ -\frac{1}{T_1} & -\frac{V_1}{T_3} & 0 & \frac{V_1}{T_3} & 0 \\ 0 & \frac{1}{T_2} & \frac{V_2}{T_2} & 0 & \frac{V_2}{T_2} \\ 0 & 0 & 0 & \frac{V_3}{T_4} & \frac{1}{T_4} \\ 0 & 0 & 0 & \frac{1}{T_5} & 0 \end{bmatrix} \begin{bmatrix} x_1(t) \\ x_2(t) \\ x_3(t) \\ x_4(t) \\ x_5(t) \end{bmatrix} + \begin{bmatrix} 0 & 0 \\ \frac{1}{T_1} & 0 \\ 0 & 0 \\ 0 & \frac{1}{T_4} \\ 0 & 0 \end{bmatrix} \begin{bmatrix} \Delta\ddot{z}(t) \\ \Delta c(t) \end{bmatrix} \tag{13}$$

$$\begin{bmatrix} \Delta\hat{\ddot{z}}(t) \\ \Delta\hat{\dot{z}}(t) \\ \Delta\hat{z}(t) \\ \Delta\hat{\dot{c}}(t) \\ \Delta\hat{c}(t) \end{bmatrix} = \begin{bmatrix} -1 & -V_1 & 0 & V_1 & 0 \\ 0 & 1 & 0 & 0 & 0 \\ 0 & 0 & 1 & 0 & 0 \\ 0 & 0 & 0 & 1 & 0 \\ 0 & 0 & 0 & 0 & 1 \end{bmatrix} \begin{bmatrix} x_1(t) \\ x_2(t) \\ x_3(t) \\ x_4(t) \\ x_5(t) \end{bmatrix} + \begin{bmatrix} 1 & 0 \\ 0 & 0 \\ 0 & 0 \\ 0 & 0 \\ 0 & 0 \end{bmatrix} \begin{bmatrix} \Delta\ddot{z}(t) \\ \Delta c(t) \end{bmatrix} \tag{14}$$

$T_1 \sim T_5$ and $V_1 \sim V_3$ are the parameters that determine the cut-off frequencies, in observing the five states, and damping.

Finally, to form and solve the system governing Equations 10, 12 and 3-6, the generalized partitioning method is employed. The procedure of the algorithm proposed in this paper follows the flow shown in Figure 6.

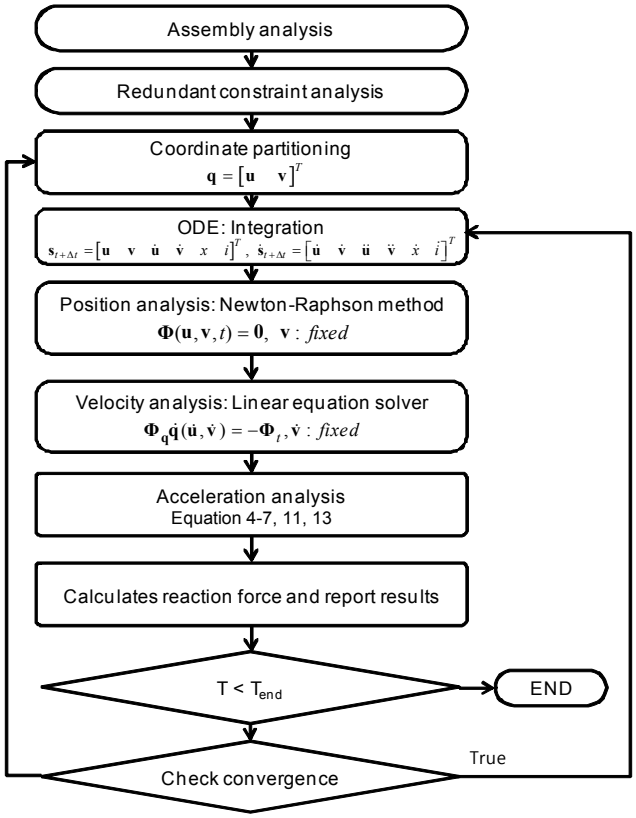

Figure 6. Numerical analysis flow

3 ANALYSISIS

To evaluate the effect of damper between Maglev vehicles on curve negotiation, vehicle motion and guiding characteristics throughout running test and simulation are analyzed. In the simulation, the 60m-radius and 180m-radius curve are arranged as listed in Table 1.

Table 1 Configurations of the curved guideway

Item	Specification	
Circular curve radius	60m	180
Cant	2°	2.5°
Velocity	20km/h	40km/h

3.1 Dynamic response on the 60m-radius curve

According to the installation inter-car damper or not, dynamic curving behaviors of the Maglev on the 60m-radius curve are simulated respectively. The maximum yawing acceleration occurs at the turning point from tangent section to transition curve and from transition curve to circular curve. As shown in

Figure 6 and 7, Yaw damper equipped for Maglev vehicle has sufficient effect when the vehicle traveling along the 60m-radius curve.

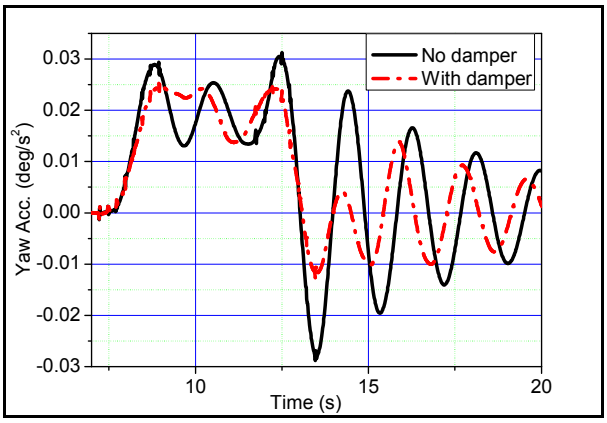

Figure 6. Yaw acceleration of Mc 1

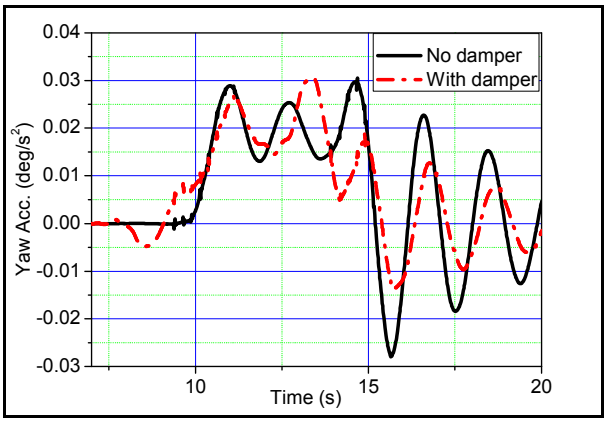

Figure 7. Yaw acceleration of Mc 2

Next, the lateral air gap responses from both in the case of with damper and without damper are compared as shown in Figure 8. Both cases show similar amplitude, and it could be stated that the vehicles travel along the 60m-radius curve within an allowable range.

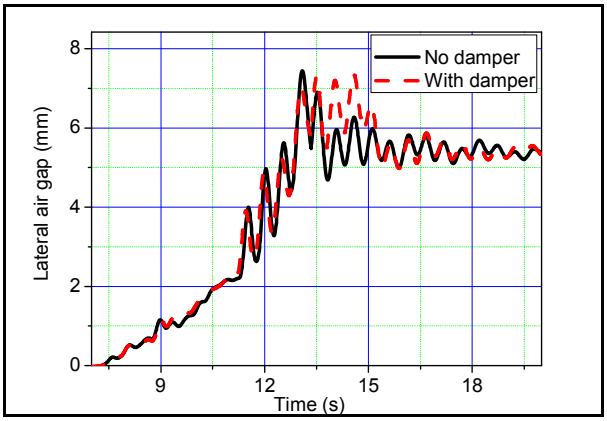

Figure 8. Lateral displacement of the bogie 4

3.2 Dynamic response on the 180m-radius curve

In this section, dynamic responses of the vehicle on the 180m-radius curve are evaluated respectively. As the simulation on the 60m-radius curve, yaw damper equipped for Maglev vehicle has sufficient effect when the vehicle traveling along the 180m-radius curve. As shown in Figure 9 and 10, yaw acceleration of Maglev vehicle equipped the damper is decreased than not equipped.

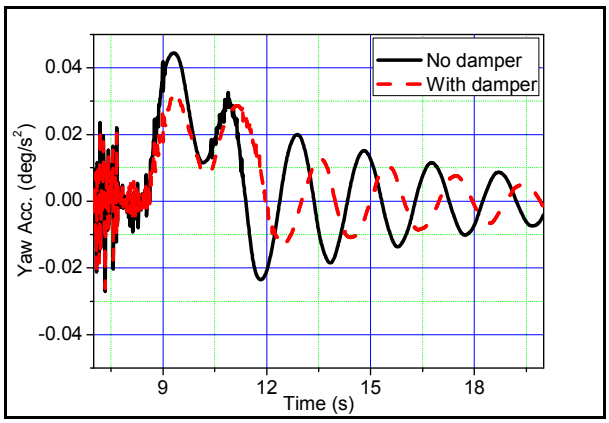

Figure 9. Yaw acceleration of Mc 1

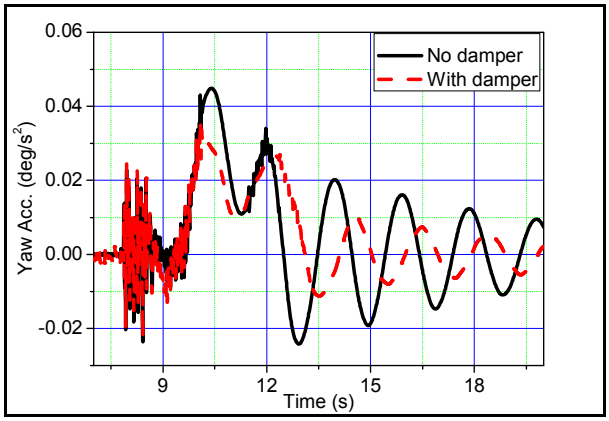

Figure 10. Yaw acceleration of Mc 2

Figure 11 shows the lateral air gap of the bogie 4, close to the position of the damper equipped. Both of cases, lateral air gap show similar deviation within an allowable range. Consequently, it can be concluded that the mechanical collision can be avoided when Maglev travels along the 180m-radius curve.

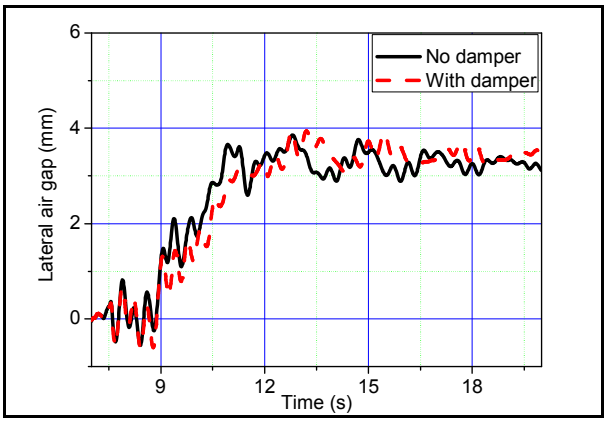

Figure 11. Lateral displacement of the bogie 4

3.3 Test results

A running test of Maglev vehicle is performed to verify the reasonableness of the simulation proposed.

A lateral vibration measured on Maglev is shown in Figure 13 and 14. As the results from simulation are compared with those of the test, it may be noted that the two sets of results are displayed similar tendency. Yaw damper has remarkable effect on attenuation in yawing of the vehicle traveling along the curve, which is evident on RMS values of the lateral acceleration which are significantly smaller than in case of without damper. Here, it is very difficult to expect that Maglev vehicle simulation will be precisely identical to the test, because the irregularities that result from surface roughness, guideway deflection are not applied to the dynamic simulation, unlike actual system. If the irregularities are applied to the dynamic model, it is believed that the simulation is similar to the test.

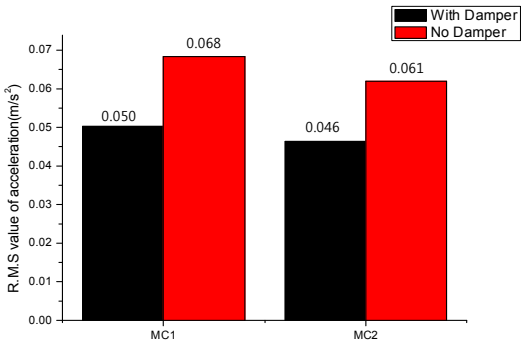

Figure 12. R.M.S Value of lateral acceleration running through test track

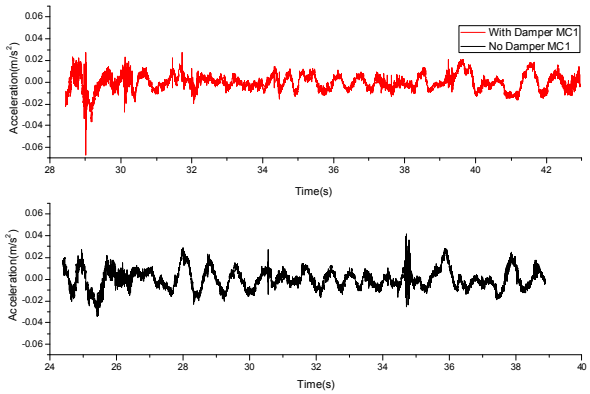

Figure 13. Lateral vibration running through test track, Mc 1

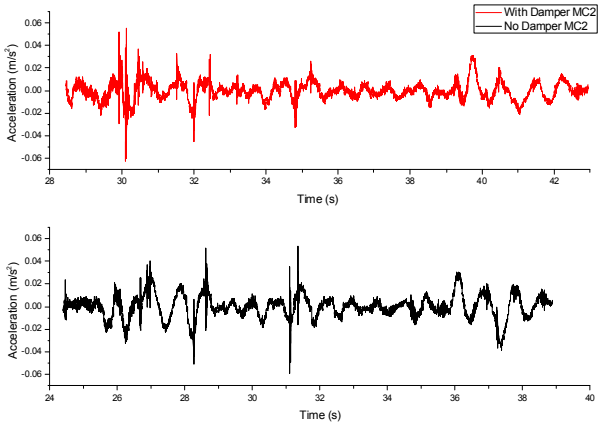

Figure 5. Lateral vibration running through test track, Mc 2

4 CONCLUSIONS

In order to provide more realistic simulation to show the effect of damper connecting two vehicles, the use of a full vehicle multibody dynamic model was presented. This dynamic model include control algorithm of the electromagnet and, levitation and guidance force. With the proposed model, yawing motion and ride quality of the vehicle levitated were analyzed while it is being driven and guided by the electromagnetic force according to the effect of damper. From the simulation results, it was clear to see that yaw damper has remarkable effect on attenuation in lateral acceleration when the vehicle travels along the curve. The results from running test are also similar. Therefore for the low speed EMS maglev vehicle mainly running in the city as urban transit, vehicle-to-vehicle damper could be recommended.

Evaluation of the results of running test and analysis assure safety and curve negotiation as transit system. In the future, further running test and analysis will be made in an attempt to improve various elements.

5 REFERENCES

Zhao, C.F., Zhai, W.M. and Wnag, K.Y., Dynamic responses of the low-speed maglev vehicle on the curved guideway, *Vehicle System Dynamics*, Vol. 38, No. 3, pp.185-210, 2002.

B.H. YIM, H.S.HAN, J.K.LEE and S.S.KIM. Curving performance simulation of an EMS-type Maglev vehicle, *Vehicle System Dynamics, Vol 47, No 10,* Oct 2009.

P.K. SINHA. *Electromagnetic Suspension Dynamics and Control*, Peter Peregrinus Ltd. London, 1987.

E.J. HAUG, *Computer-aided Kinematics and Dynamics of Mechanical System*, Allyn and Bacon, USA, 1986.

SUNG.H.K., JUNG, B.S., CHO, J.M., JANG, S.M., LEE, J.M., AND CHO, H.J., Magnetic levitation control using DSP TMS320LF2407. In: *Proceedings of the KIEE Summer Conference,* 2004, pp.1340-1342.

ANDERSON, R.J., *A'GEM Rail Vehicle Dynamics Software Package user's manual,* R.J Anderson Engineering Analysis,1994